Title:	A Recursive Park Transformation to Improve the Performance of Synchronous Reference Frame Controllers in Shunt Active Power Filters
Authors:	Alberto Pigazo, *Member, IEEE*, Víctor M. Moreno, *Member, IEEE* and Emilio J. Estébanez
Publication:	IEEE Transactions on Power Electronics, vol. 24, no. 9. September 2009. pp. 2065-2075.
D.O.I.:	10.1109/TPEL.2009.2025335

A Recursive Park Transformation to Improve the Performance of Synchronous Reference Frame Controllers in Shunt Active Power Filters

Alberto Pigazo, *Member, IEEE*, Víctor M. Moreno, *Member, IEEE* and Emilio J. Estébane

***Abstract*— Load harmonic currents and load unbalances reduce power quality (PQ) supplied by electrical networks. Shunt Active Power Filters (SAPFs) are a well-known solution which can be employed to enhance electrical PQ by injecting a compensation current at the point of common coupling (PCC) of the SAPF, the load and the electrical grid. Hence, SAPF controllers must determine the instantaneous values of the compensation reference current, including non-desirable components of the load current. A family of SAPF controllers, which evaluates the compensation reference current using synchronous rotating frames (SRFs), employs a structure based on Park Transformations: direct transform, Low-Pass Filtering (LPF) and inverse transform. The cut-off frequency and the filter order of the LPF stage must be properly designed in order to obtain an accurate reference current and a fast dynamic response of these SAPF controllers.**

This paper proposes a recursive implementation of the direct Park Transformation which avoids the filtering stage and allows accurate SRF controllers to be designed. Moreover, the proposed implementation is non-dependant on PCC conditions. The proposed implementation is evaluated using a three-phase three-wire SAPF and compared with LPF based controllers by simulation and experimentally.

I. Introduction

Shunt active power filtering is a well-known technique employed to compensate load harmonic currents, load unbalance or load reactive power at the PCC of the SAPF, the electrical grid and the distorting load [1] [2]. A digital SAPF controller must carry on three functionalities during each sampling interval: evaluate the instantaneous values of the compensation reference current; evaluate the current consumption which is maintained by the SAPF dc-bus voltage; and ensure that the injected compensation current at the PCC matches the previously evaluated values [3]. The performance of the SAPF depends on each of these three functionalities, with the instantaneous evaluation of the compensation reference current being a key point.

The reference current can be evaluated using different approaches [2][4], the most commonly used are: the calculation of the load active and reactive power, e.g. the pq method [5]-[7] or the FBD method [8][9]; the direct evaluation of the load active current, such as SRF decomposition based methods [10]-[12]; or the evaluation of the load current harmonic components for selective compensation, e.g. discrete Fourier transform (DFT) [13][14] or Kalman filtering [15][16]. This paper focuses on single SRF based methods for harmonic currents compensation, where the compensation reference current $i^*_{\alpha\beta}(k)$ can be evaluated by subtracting the target source current $\hat{i}_{\alpha\beta}(k)$ from the load current $i_{\alpha\beta}(k)$ (fig. 1.a). If selective harmonic compensation is required, more SRFs should be employed in order to establish the harmonic components of the source target current. The basic structure of SRF methods, depicted in fig. 1.b, consists of direct DQ and inverse DQ^{-1} Park Transformations, which allow the evaluation of a specific harmonic component of the input signal $i_{\alpha\beta}(k)$, and a low-pass filtering stage LPF.

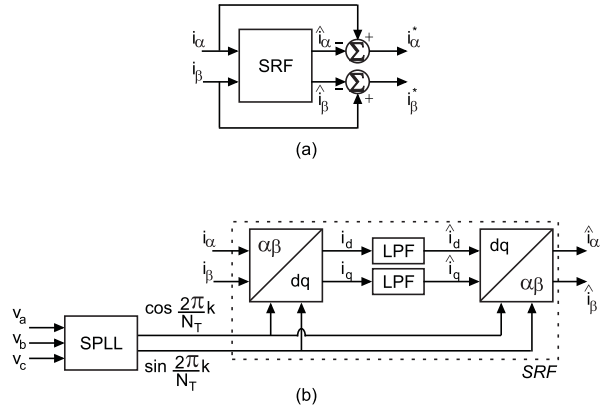

Fig. 1. a) Evaluation of the compensation reference current based on SRF methods and b) the general structure of the SRF methods

The software phase-locked-loop (SPLL) generates $\sin\omega k$ and $\cos\omega k$ functions, where $\omega = \frac{2\pi}{N}$ and $N \in \mathcal{R}^+$ is the number of samples which should be considered at the fundamental grid frequency, synchronized with the fundamental component of the grid voltage. These signals can be applied to $i_{\alpha\beta}(k)$ through the direct Park Transformation (DQ) in order to obtain a frequency shifting effect of the harmonic components of the load current. The DQ transformation output signals depend on the load current spectrum (harmonic frequency and sequence) and the performance of the SPLL. The harmonic component matching the SRF pulsation (ω) is shifted to a dc component while other frequency components of the input signal are shifted to higher frequencies, i.e. 5^{th} and 7^{th} harmonics to 6ω. Hence, the input signal components with frequency ω can be obtained after a low-pass filtering stage applied to the DQ transformation outputs. Finally, the

A. Pigazo, V. M. Moreno and E. J. Estébanez are with the Dept. of Electronics and Computers, University of Cantabria, Santander, 39004 Spain (phone:+34-942-201338; fax:+34-942-201303; emails: pigazoa@unican.es, morenov@unican.es, estebanezej@unican.es).

DQ^{-1} transformation allows the target source current in $\alpha\beta$ coordinates to be obtained. As a consequence, the low-pass filtering stage must be designed carefully (cut-off frequency and filter order) in order to avoid erroneous compensation reference signals during the SAPF operation. In particular, the load current spectrum must be considered during the design process.

This paper presents a recursive implementation of the DQ transform, DQ_r, which avoids the low-pass filtering stage in SRF based structures. This implementation allows an accurate evaluation of specific harmonic components independent of PCC conditions. The mathematical analysis, simulation and experimental results obtained on a three-phase three-wire SAPF are given.

II. SRF BASED CONTROLLERS IN THE FREQUENCY DOMAIN

This section analyzes the frequency response of the structure shown in fig. 1.b. and proposes a first approach to the recursive implementation of the Park Transformation DQ_r. As will be shown in this section, this approach is sensitive to frequency variations and a modified DQ_r will be proposed.

A. DQ-LPF-DQ^{-1} structure

The Park Transformation allows the load current signals to be represented using a rotating complex frame. The Park Transformation is described as:

$$\begin{pmatrix} x_d \\ x_q \end{pmatrix}_k = \mathbf{\Phi}_k \begin{pmatrix} x_\alpha \\ x_\beta \end{pmatrix}_k \tag{1}$$

where:

$$\mathbf{\Phi}_k = \begin{pmatrix} cos(\omega k) & sin(\omega k) \\ -sin(\omega k) & cos(\omega k) \end{pmatrix} \tag{2}$$

with $x_\alpha(k)$ and $x_\beta(k)$ being the load current components in a stationary complex frame (i.e. outputs of a Clarke Transformation), $x_d(k)$ and $x_q(k)$ the outputs of the Park Transformation and $\mathbf{\Phi}_k$ the transformation matrix obtained by means of the SPLL. The harmonic components of the load current can be filtered-out from $x_d(k)$ and $x_q(k)$ by applying a LPF filtering stage:

$$H_{LPF}(z) = \frac{\sum_{i=0}^{m} n_i z^i}{\sum_{i=0}^{m} d_i z^i} \tag{3}$$

with m being the filter order and n_i and d_i constant coefficients corresponding to the numerator and denominator respectively. Butterworth filters are commonly employed in the filtering stage due to their plain gain up to the cut-off frequency.

Finally, the $\alpha\beta$ coordinates of the fundamental component of the load current at ω can be obtained by applying the inverse Park Transformation:

$$\begin{pmatrix} \hat{x}_\alpha \\ \hat{x}_\beta \end{pmatrix}_k = \mathbf{\Phi}_k^{-1} \begin{pmatrix} \hat{x}_d \\ \hat{x}_q \end{pmatrix}_k \tag{4}$$

where $\hat{x}_d(k)$ and $\hat{x}_q(k)$ are the filtered outputs of the DQ transformation.

The DQ-LPF-DQ^{-1} transformation can be analyzed in the frequency domain [17]-[20] obtaining:

$$\hat{x}_\alpha(z) = G_1(z)x_\alpha(z) - G_2(z)x_\beta(z) \tag{5}$$
$$\hat{x}_\beta(z) = G_2(z)x_\alpha(z) + G_1(z)x_\beta(z) \tag{6}$$

where:

$$G_1(z) = \frac{1}{2}\left[H_{LPF}\left(e^{j\omega}z\right) + H_{LPF}\left(e^{-j\omega}z\right)\right] \tag{7}$$

$$G_2(z) = \frac{j}{2}\left[H_{LPF}\left(e^{j\omega}z\right) - H_{LPF}\left(e^{-j\omega}z\right)\right] \tag{8}$$

B. Proposed DQ_r-DQ^{-1} structure

The direct Park Transformation and the low pass filtering stage can be implemented by applying a recursive algorithm. The average values of the DQ transform outputs at instants k and $k-1$ can be obtained by considering $N_r \in \mathcal{Z}^+$ samples at the fundamental grid frequency:

$$\begin{pmatrix} \hat{x}_d \\ \hat{x}_q \end{pmatrix}_k = \frac{1}{N_r} \sum_{n=k-N_r+1}^{k} \mathbf{\Phi}_n \begin{pmatrix} x_\alpha \\ x_\beta \end{pmatrix}_n \tag{9}$$

$$\begin{pmatrix} \hat{x}_d \\ \hat{x}_q \end{pmatrix}_{k-1} = \frac{1}{N_r} \sum_{n=k-N_r}^{k-1} \mathbf{\Phi}_n \begin{pmatrix} x_\alpha \\ x_\beta \end{pmatrix}_n \tag{10}$$

As a consequence, the recursive Clark Transformation can be obtained:

$$\begin{pmatrix} \hat{x}_d \\ \hat{x}_q \end{pmatrix}_k = \begin{pmatrix} \hat{x}_d \\ \hat{x}_q \end{pmatrix}_{k-1} + \frac{1}{N_r}\mathbf{\Phi}_k \begin{pmatrix} \Delta\left(x_\alpha, N_r\right) \\ \Delta\left(x_\beta, N_r\right) \end{pmatrix}_k \tag{11}$$

where:

$$\Delta\left(x_\alpha, N_r, k\right) = x_\alpha(k) - x_\alpha(k-N_r) \tag{12}$$
$$\Delta\left(x_\beta, N_r, k\right) = x_\beta(k) - x_\beta(k-N_r) \tag{13}$$

As in the previous case, the $\alpha\beta$ coordinates of the fundamental component of the load current can be obtained by applying (4). It must be considered that, depending on the sampling frequency and the fundamental grid frequency ω, the number of samples employed for the recursive implementation N_r can be different from N, which is evaluated by the SPLL: The pulsation of sin and cos functions ($\frac{2\pi}{N}$) is changed by the SPLL to maintain the synchronization with the grid voltage. The next section discusses the effect of $N \neq N_r$ on this implementation.

Appendix I analyzes the recursive Park transformation in the frequency domain, obtaining:

$$\hat{x}_\alpha(z) = G_{1,r}(z)x_\alpha(z) - G_{2,r}(z)x_\beta(z) \tag{14}$$
$$\hat{x}_\beta(z) = G_{2,r}(z)x_\alpha(z) + G_{1,r}(z)x_\beta(z) \tag{15}$$

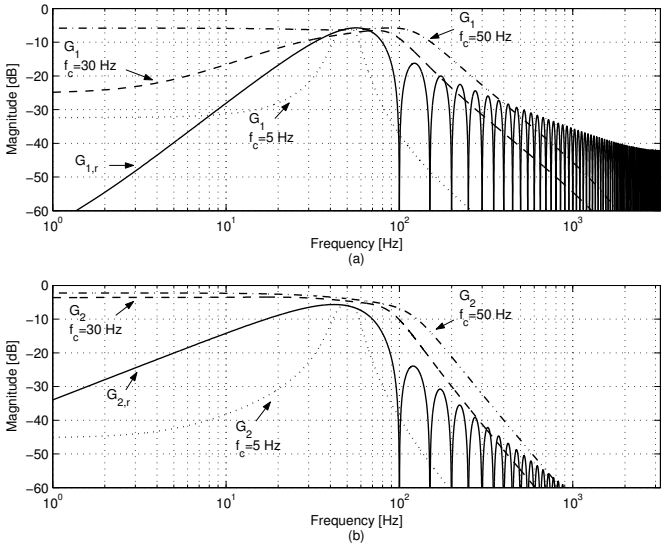

Fig. 2. Frequency responses of a) G_1 and $G_{1,r}$ and b) G_2 and $G_{2,r}$. $N = N_r = 128$

with:

$$G_{1,r}(z) = \frac{\left(z^{N_r} - 1\right)(z - cos\omega)}{N_r\left(z^{N_r+1} - 2cos\omega z^{N_r} + z^{N_r-1}\right)} \quad (16)$$

$$G_{2,r}(z) = \frac{\left(z^{N_r} - 1\right) sin\omega}{N_r\left(z^{N_r+1} - 2cos\omega z^{N_r} + z^{N_r-1}\right)} \quad (17)$$

C. Frequency domain analysis of the SRF structures

Fig. 2 compares the frequency responses of DQ-LPF-DQ^{-1} and DQ_r-DQ^{-1} transformations through the analysis of the obtained transfer functions: $G_1(z)$ and $G_{1,r}(z)$ (fig. 2.a) and $G_2(z)$ and $G_{2,r}(z)$ (fig. 2.b). The analyzed LPF based implementations consist of 2^{nd} order Butterworth filters with 5, 30 and 50 Hz cut-off frequencies:

$$H_{5Hz}(s) = \frac{987}{s^2 + 44.43s + 987} \quad (18)$$

$$H_{30Hz}(s) = \frac{35530.6}{s^2 + 266.6s + 35530.6} \quad (19)$$

$$H_{50Hz}(s) = \frac{98696.0}{s^2 + 444.3s + 98696.0} \quad (20)$$

As can be seen in fig. 2.a, $G_1(z)$ and $G_{1,r}(z)$ reach a $-6\ dB$ maximum gain, which is due to the fact that both x_α and x_β components contribute to the averaged outputs $\hat{x}_\alpha$ and $\hat{x}_\beta$. The LPF based method with a 5 Hz cut-off frequency presents the narrowest band-pass at the fundamental grid frequency but, as will be shown in the following sections, its response time under load transients is the worst. Needing a narrow band-pass in order to compensate the load current harmonics properly, slow response times can be considered as a drawback when the current harmonics of time-varying non-linear loads are compensated. The frequency response of G_1 with $f_c = 50\ Hz$ is the worst due to the fact that the attenuation for the 3^{rd} and 5^{th} harmonics is low, reaching -9.74 and $-19.25\ dB$ gains respectively. Moreover, the plain gain response below 50 Hz does not allow low frequency load variations to be filtered out. The LPF based method with $f_c = 30\ Hz$ can be an alternative for filtering out the 5^{th} harmonic (its effect is reduced to 5% of its initial value) but the 3^{rd} harmonic remains high ($-17\ dB$) and it can not be employed in four-wire configurations with high load current consumption at 150 Hz. As a consequence, depending on the load current spectrum, which can vary with the PCC voltage distortion, the LPF must be properly designed, reaching a compromise between the band-pass width of $G_1(z)$ and the response time under dynamical load conditions. The proposed method, as will be shown in the following sections, has a constant response time and its frequency response ($G_{1,r}(z)$) allows undesirable harmonic components of the load current to be compensated by introducing zeros at their frequencies.

Fig. 2.b shows the frequency response obtained for $G_2(z)$ and $G_{2,r}(z)$. Again the LPF with $f_c = 5\ Hz$, despite being the slowest one, obtains the narrowest band-pass at the pulsation of the SRF. The dynamic response can be improved by increasing the cutoff frequency but, then, the band-pass frequencies around ω increases and, hence, the impact of harmonics different from the fundamental component increases. The effect of these load current harmonics can be minimized by means of the proposed recursive Park Transformation, which introduces multiple notches in the frequency response at their frequencies.

According to (14)-(17), the proposed recursive implementation is sensitive to frequency variations of the fundamental grid component. Rewriting (16) in a zero-pole form:

$$G_{1,r}(z) = \frac{1}{N_r} \cdot \frac{z - cos\omega}{z} \cdot \frac{\prod_{i=0}^{N_r-1} z - e^{j\frac{2\pi}{N_r}i}}{(z - e^{j\omega})(z - e^{-j\omega})} \quad (21)$$

In case $N_r = N$, $\omega = \frac{2\pi}{N} = \frac{2\pi}{N_r}$ and two zeros in the numerator, at ω, are cancelled due to the poles in the denominator. Under $N_r \neq N$, such zero-pole compensation can not be done and, as a consequence, a resonance around ω would appear in the frequency response. Moreover, due to the effect of non compensated zeros at $\frac{2\pi}{N_r}$, a notch should be present in the frequency response at $\frac{2\pi}{N_r}$. An equivalent analysis can be carried out in case of $G_{2,r}$. This effect is analyzed in fig. 3 by plotting $G_{1,r}$ at different sampling frequencies ($f_s = 6.4\ kHz$ and $f_s = 1\ kHz$) and grid frequencies (49, 50 and 51 Hz). From fig. 3.a and 3.c, the frequency response of the proposed method is little dependent on the sampling frequency being the gain at very low frequencies the main difference($-67.13\ dB$ at $f_s = 6.4\ KHz$ and $-51.71\ dB$ at $f_s = 1\ KHz$). Hence, the proposed recursive implementation can be considered an interesting alternative in SAPF controllers operating at low switching frequencies to reduce the switching losses. Due to the effect of grid frequency variations the zero of $G_{1,r}$ can not compensate for the transfer function poles at the SRF pulsation ω and, as a consequence, gain peaks appear around the SRF frequency. This phenomenon is shown in more detail in fig. 3.b and 3.d. As can be seen, the magnitude of the gain peaks depends on the deviation of N_r from N.

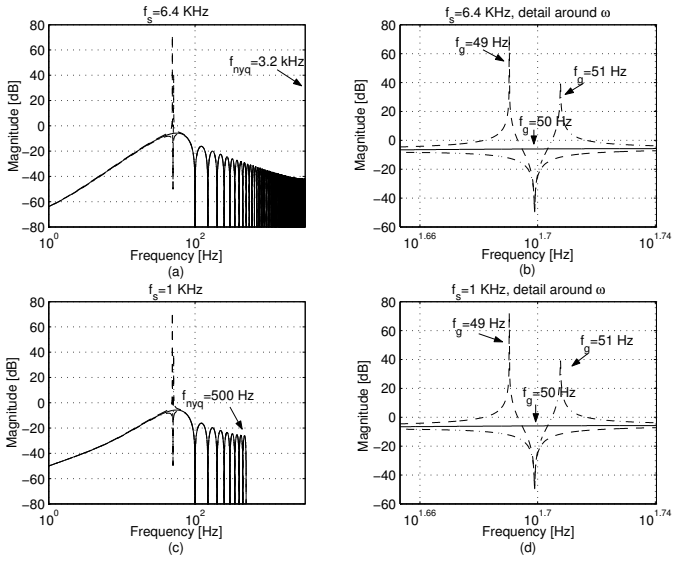

Fig. 3. Frequency response of $G_{1,r}(z)$ for different fundamental grid and sampling frequencies a) $f_s = 6.4\ kHZ$, b) detail around ω at $f_s = 6.4\ KHz$, c) $f_s = 1\ KHz$ and d) detail around ω at $f_s = 1\ KHz$

D. Modified recursive Park Transformation

In order to avoid the effect of grid frequency variations on the proposed recursive transformation two alternatives can be employed: a) The sampling frequency of the overall controller can be changed to match $N = N_r$ or b) the frequency drift effect can be compensated by software. The first solution implies a dynamic redesign process of other elements of the SAPF controller in order to maintain their performance. This is the case of PI dc-bus voltage controllers where the proportional and integral constants should be changed to ensure the SAPF stability and compensation capability [21]. As a consequence, the second alternative has been selected.

Grid frequency variations are tracked by means of the SPLL, which changes the elements of the transformation matrix $\mathbf{\Phi}$. As a consequence, and according to (21), resonances and notches in fig. 3 are due to Δ operators in (12) and (13). In order to place properly the zeros in (21), the averaging windows corresponding to Δ operators must be dynamically resized each sampling interval. Anyway, it must be considered that only an integer number of samples N' can be applied to Δ operators while N can be non-integer and, as a consequence, small frequency drifts can remain reducing the method performance. Their effect can be compensated by applying a new transformation matrix, which can be interpreted as a transformation of $\alpha\beta$ components to a second rotating frame whose pulsation corresponds to N'. In this way, the poles in (21) at ω are shifted to the frequency of the previously displaced zeros and zero-pole compensation success again. Hence, the modified Park transformation can be defined as:

$$\begin{pmatrix} \hat{x}_d \\ \hat{x}_q \end{pmatrix}_k = \begin{pmatrix} \hat{x}_d \\ \hat{x}_q \end{pmatrix}_{k-1} + \frac{1}{N'}\mathbf{\Theta}_k \begin{pmatrix} \Delta\left(x_\alpha, N'\right) \\ \Delta\left(x_\beta, N'\right) \end{pmatrix}_k \quad (22)$$

where

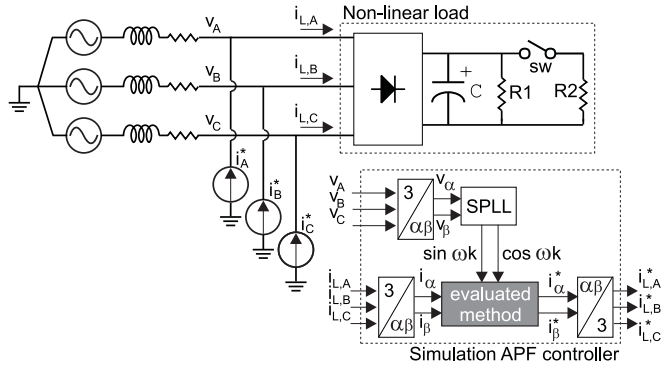

Fig. 4. Simulation model

$$N' = round\left(\frac{1}{f_{PLL}T_s}\right) \quad (23)$$

with T_s being the sampling period, f_{PLL} the measurement of the grid frequency obtained by means of the SPLL and

$$\mathbf{\Theta}_k = \mathbf{\Phi}_k \begin{pmatrix} cos\left(\omega_\epsilon k\right) & sin\left(\omega_\epsilon k\right) \\ -sin\left(\omega_\epsilon k\right) & cos\left(\omega_\epsilon k\right) \end{pmatrix} \quad (24)$$

$$\omega_\epsilon = 2\pi\left(\frac{1}{N'T_s} - f_{PLL}\right) \quad (25)$$

In order to obtain the $\alpha\beta$ coordinates of the fundamental component of the load current the inverse Park Transformation must be modified:

$$\begin{pmatrix} \hat{x}_\alpha \\ \hat{x}_\beta \end{pmatrix}_k = \mathbf{\Theta}_k^{-1} \begin{pmatrix} \hat{x}_d \\ \hat{x}_q \end{pmatrix}_k \quad (26)$$

III. Simulation Results

The SRF based controller depicted in fig. 1.a has been implemented in MatLab/Simulink in order to establish its performance when DQ-LPF-DQ^{-1}, DQ_r-DQ^{-1} and modified DQ_r-DQ^{-1} transformations are employed. The implementations based on LPFs apply 2^{nd} order Butterworth low-pass filters with cutoff frequencies $f_c = 5\ Hz$ and $f_c = 50\ Hz$. The controller sampling frequency is $f_s = 6.4\ KHz$. The simulation results have been obtained considering that the controller under test is applied to an ideal SAPF, without dc-bus voltage and injection current controllers, and, hence, the injection current matches the compensation reference current (fig. 4). Moreover, it is considered that only harmonic compensation is required (no reactive power compensation). The employed test load is a three-phase three-wire full-wave diode rectifier with capacitive dc side which is fed by a distorted PCC voltage according to IEEE Std. 519 [22] ($3\%\ 5^{th}$ and $3\%\ 7^{th}$ harmonics). The load dc-side characteristics can be changed during the tests in order to evaluate the dynamic response and the performance of each method. The analyzed SRF implementations have been tested under slow frequency variations of the grid voltage (different N_r and N) and without frequency variations (N_r equals N) in order to establish their performance.

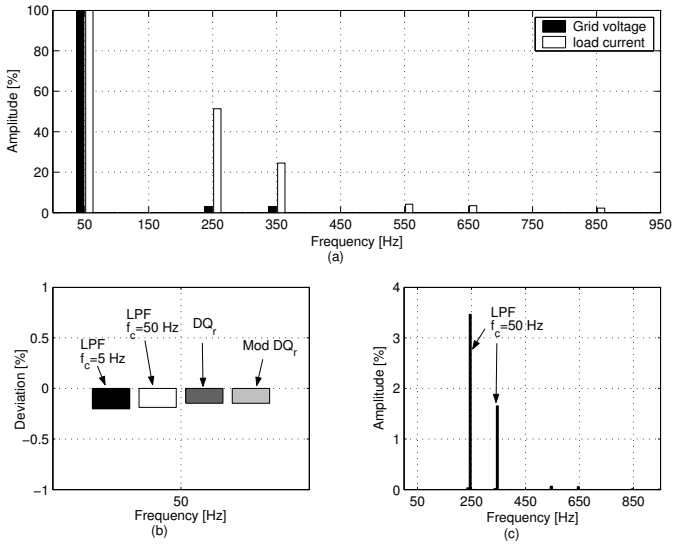

Fig. 5. Compensation results in stationary state. a) Grid voltage and load current ($V_{base} = 20\ V_{rms}$, $I_{base} = 3.16\ A$ in phase A), b) deviation from the fundamental component of the source current and c) amplitude of the harmonic components of the source current

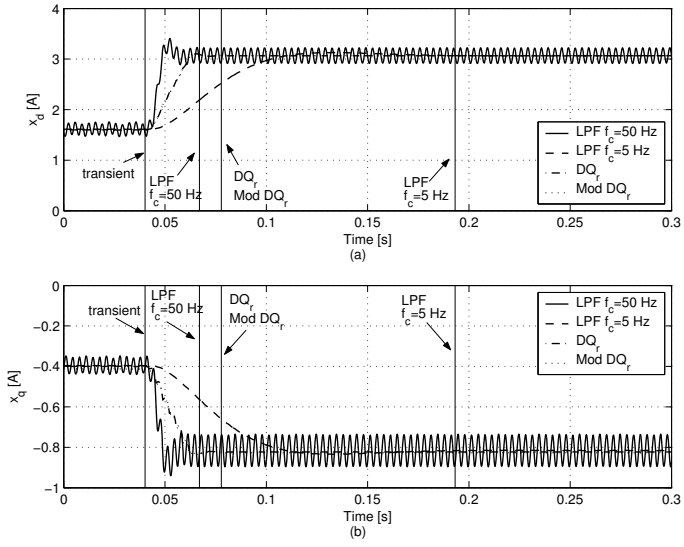

Fig. 6. Response to a load transient. a) d and b) q components of each SRF based controller

A. N_r equals N

The grid frequency is maintained at $50\ Hz$ ($N = N_r = 128$) during the test and the performance of each method is evaluated in abc and dq components. The spectra of the applied source voltage and the load current signals in phase A are shown in f g. 5.a, where the total harmonic distortion (THD) of the load current is $57.4\ \%$, with high 5^{th} and 7^{th} harmonics.

Once the SAPF begins the compensation of the load current harmonics, the source current consumption at the fundamental grid component must be maintained under the simulation model depicted in f g. 4. The obtained results demonstrate that the deviation of the source current from the load current at the fundamental grid frequency is maintained within a maximum $0.2\ \%$ (f g. 5.b) due to the employed ideal SAPF model.

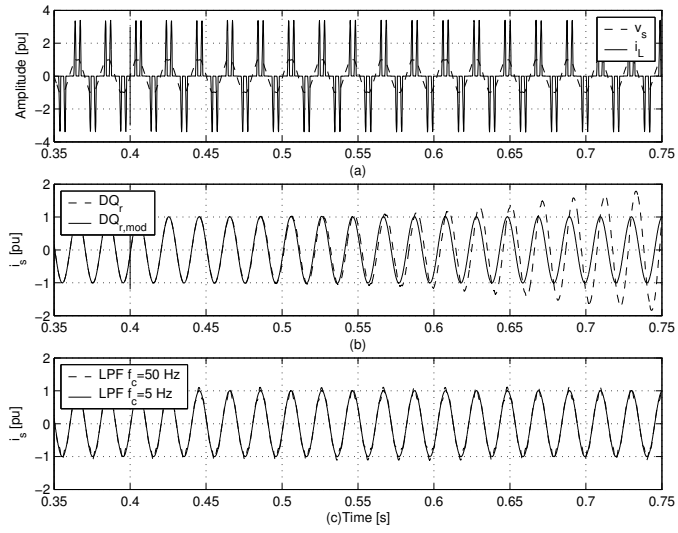

Fig. 7. SRF based SAPF controllers with a frequency variation. a) PCC voltage v_s and load current i_L in phase A, b) recursive and modif ed recursive DQ and c) LPF based implementations. $V_{base} = 20\ V_{rms}$, $I_{base} = 3.16\ A$

The measured source current harmonics are shown in f g. 5.c and, as can be seen, the SRF method based on the LPF with $f_c = 50\ Hz$ shows the worst performance due to the frequency response of this method. In this case, the 5^{th} and 7^{th} load current harmonics are only attenuated up to $3.5\ \%$ and $1.7\ \%$.

In order to test the performance of the SRF controllers the load current consumption changes at $0.04\ s$, reaching a new steady state after $22.97\ ms$. During the load transient the PCC voltage maintains its harmonic distortion levels. The inner dq components of each SRF controller are shown in f g. 6.a and 6.b. The measured response times applying the recursive implementations are equivalent ($T_r = 37.66\ ms$) while the $f_c = 50\ Hz$ LPF based method is the fastest one, with $T_r = 26.87\ ms$, and the SRF controller with a $f_c = 5\ Hz$ LPF is the slowest one ($T_r = 153.2\ ms$). Moreover, due to the effect of the LPF both x_d and x_q have ripple, $9.90\ \%$ and $19.13\ \%$ respectively for $f_c = 50\ Hz$ and a low $0.1\ \%$ and $0.2\ \%$ respectively for $f_c = 5\ Hz$. As a consequence, both stationary and dynamic responses have a high dependency on the employed LPF characteristics in such SRF based controllers.

B. Different N_r and N

Section II.C shows that grid frequency variations reduce the performance of the proposed recursive implementation. Hence, the SRF implementations have been analyzed under slow grid frequency variations ($N_r = 128$ depends on the assumed grid and sampling frequencies while N is determined by the SPLL). Per unit grid voltage and load current during a frequency variation are shown in f g. 7.a. The frequency varies from $50\ Hz$ at $0.4\ s$ to $49\ Hz$ at $0.6\ s$. Due to the effect discussed in section II.C, the recursive implementation fails when compensating the load current and, as a result, the source current increases with time (f g. 7.b). The modif ed recursive implementation operates properly and maintains the source current THD below $0.3\ \%$. The response of the LPF based

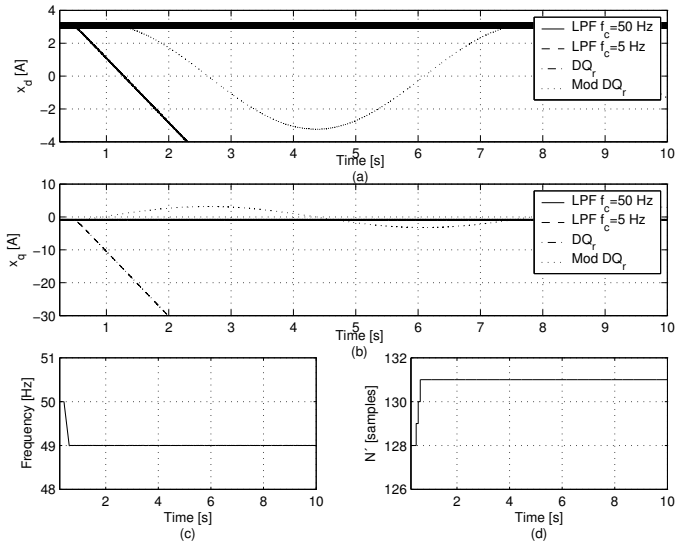

Fig. 8. SRF based SAPF controllers with a frequency variation. a) d and b) q components of each SRF based controller, c) the SPLL frequency measurement and d) dynamical resize of Δ operators (N')

implementations is shown in fig. 7.c and, as in section III.A, the performance depends on the LPF stage characteristics obtaining a source THD equal to 8.6 % in case of $f_c = 50$ Hz and 0.3 % for $f_c = 5$ Hz. As a consequence, the proposed modified recursive implementation can be considered an alternative to LPF based implementations in electrical grids with frequency variations.

Fig. 8 shows the dq components of each evaluated SRF method. Considering LPF based implementations, the obtained results in this case and $N_r = N$ are similar. In case of the recursive implementations, fig. 8.a and 8.b show that the dq components of the DQ_r method diverge and, as a consequence, the results shown in fig. 7.b are obtained. In case of the modified DQ_r method, the obtained dq components are pure sinusoids whose frequency is $\frac{\omega_\epsilon}{2\pi}$. This is due to the transformation to a second rotating frame. The SPLL measures the grid frequency (fig. 8.c) and the window length (N') is dynamically resized (fig. 8.d). The oscillation in fig. 8.a and 8.b is due to the remaining small frequency drift, which is compensated by means of the modified transformation matrix (24). As a consequence, the amplitude and frequency of these sinusoidal signals depend on the characteristics of the load current but, also, on the value of N'.

IV. Experimental Results

The analyzed SRF based controllers have been tested using a laboratory setup whose structure is depicted in fig. 9. A modified $VLT - 5004$ drive from Danfoss is employed as power stage of the three-phase three-wire SAPF and three inductors ($L = 3$ mH and $R = 1.3$ Ω) operate as current links. A power generator ($HP - 6834 - B$) is employed to generate the harmonic distortion levels according to IEEE Std. 519 [22] (3% 5^{th} and 3% 7^{th} harmonics) and feeds a full-wave diode rectifier with capacitive dc side ($C = 2200$ μF, $R_1 = 32$ Ω and $R_2 = 64$ Ω). A switch sw is employed to

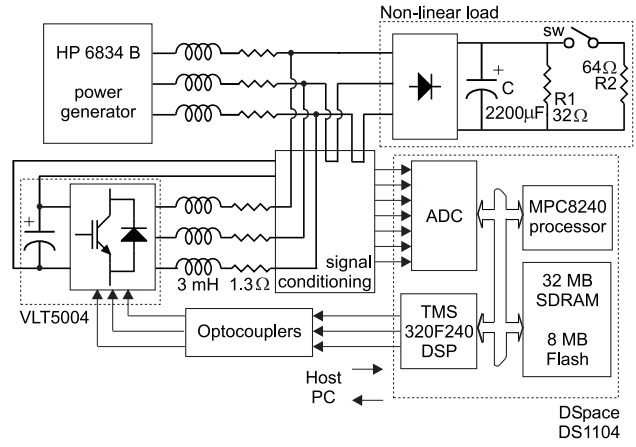

Fig. 9. Laboratory setup

generate load transients. The SAPF controller is executed in a control card $DS - 1104$ from Dspace.

A. SAPF controller implementations

The SAPF controllers previously analyzed by simulation has been experimentally implemented in order to compare their performance. The general structure of the developed controller is shown in fig. 10. As can be seen, the evaluated methods share the same general structure: a SPLL, the dc-bus controller, the injection current controller and a pulse width modulator (PWM).

The measured grid voltages are normalized in order to obtain $v_{\alpha\beta}$ signals, which will be applied to the SPLL for synchronization purposes. Normalization is required in order to avoid the impact of the grid voltage amplitude on the inner PI controller gains. The SPLL input signals are transformed to a certain rotating frame whose frequency ω_{PLL} and phase are adjusted by applying a PI controller ($t_{set} = 20$ ms and $\xi = 0.707$) to the q component of the normalized input voltage signals [23][24]. As a result, the grid voltage frequency f_{PLL}, only required by the modified $DQ_r - DQ^{-1}$ method, and the rotation matrix $\mathbf{\Phi}$ are obtained. In case of voltage unbalance, the SPLL structure should be modified in order to track the positive sequence of the grid voltage.

A PI controller allows the SAPF dc-bus voltage V_{dc} to be maintained almost constant at V_{dc}^* during the SAPF operation ensuring a proper dynamical response under load variations ($V_{dc}^* = 210$ V, $K_p = 0.024$ and $K_i = 0.011$)[21]. In order to minimize the effect of transients on the integral part of the PI controller, i.e. during the SAPF start-up, an anti-windup block has been included. The current consumption which maintains the dc-bus voltage is evaluated by multiplying the PI controller output and the sin cos signals generated by the SPLL.

The current controller must ensure that the injection current $I_{\alpha\beta}^c$ matches the compensation reference current. In this case, and due to the frequency spectrum of the non-linear load to be compensated, one proportional ($K_p = 16.5$) and three resonant blocks, with resonance frequencies at the fundamental component and the 5^{th} and 7^{th} harmonics ($K_1 = 10^3$, $K_5 = 2 \cdot 10^3$ and $K_7 = 5 \cdot 10^3$), have been selected as current controllers. It

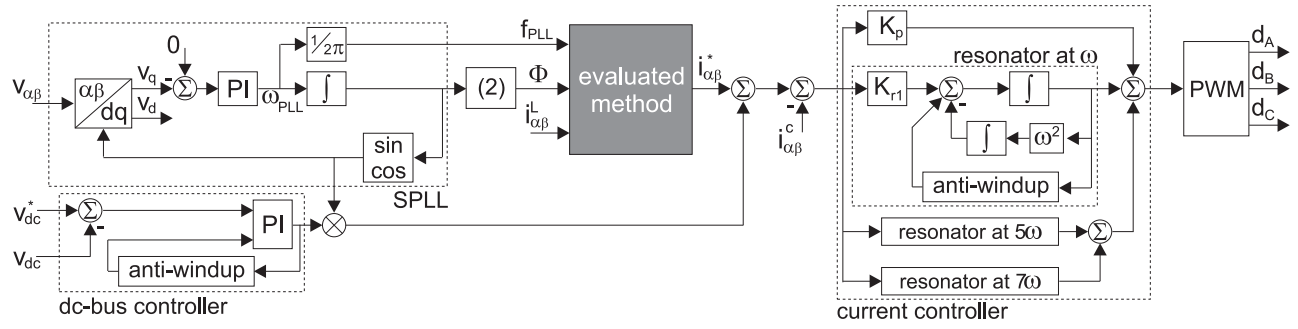

Fig. 10. Block diagram of the experimentally tested SAPF controllers

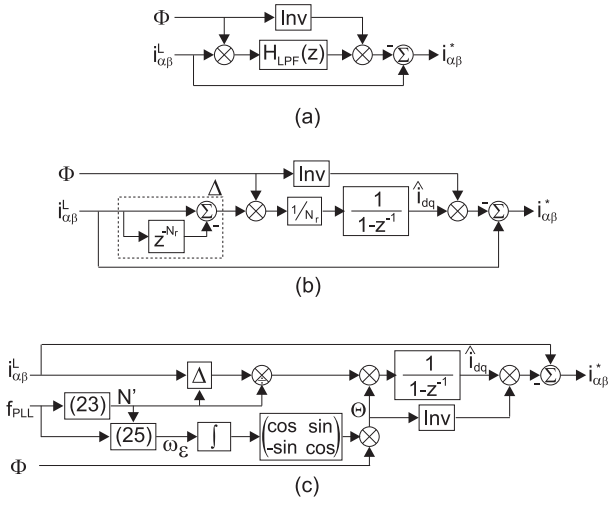

Fig. 11. Structure of the evaluated methods: a) $DQ - LPF - DQ^{-1}$, b) $DQ_r - DQ^{-1}$ and c) modified $DQ_r - DQ^{-1}$

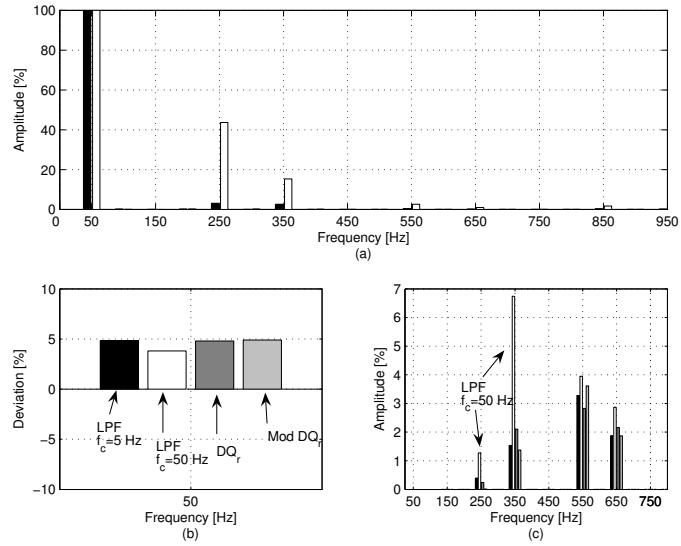

Fig. 12. Compensation results in stationary state. a) Grid voltage and load current ($V_{base} = 20\ V_{rms}$, $I_{base} = 2.21\ A$) in phase A, b) deviation from the fundamental component of the source current and c) amplitude of the harmonic components of the source current

must be considered that, if the frequency spectrum of the non-linear load current contains more harmonic orders, the number of applied resonant blocks should be increased in order to introduce new resonances at at such harmonic frequencies. The inclusion of new resonant blocks, if required, could deteriorate the controller stability and, hence, the resonant block gains should be redesigned. Moreover, it must be considered that grid frequency variations can deteriorate the performance of such current controllers based on resonant blocks. Detailed information about the implementation of current controllers based on resonant blocks can be found in [25]-[29]. The structure of the implemented current controller is depicted in fig. 10.

The current controller output signals must be applied to the modified $VLT - 5004$ drive by means of the DSP timers, which is done by evaluating the duty cycle of each inverter leg through a sinusoidal pulse width modulator [30]. The switching frequency of the SAPF is $4\ kHz$ ($N_r = 80$).

The inner structure of the evaluated methods is shown in fig. 11. In fig. 11.a the structure of a conventional $DQ - LPF - DQ^{-1}$ based method is depicted. The tested LPFs, according to (3), have been implemented as discrete 2^{nd}-order Butterworth filters with $5\ Hz$ and $50\ Hz$ cut-off frequencies. The structure of the implemented recursive Park transformation is shown in fig. 11.b. Both Δ operators are implemented as constant-length circular buffers and $\hat{x}_{dq}$ are obtained by means of two discrete integrators. The implementation of the modified $DQ_r - DQ^{-1}$ method requires the measurement of the grid frequency f_{PLL} in order to establish the window length N' of Δ operators. As a consequence, two circular buffers with variable length have been employed. The maximum and minimum length is bounded by the grid frequency limits. The obtained values are transformed to a rotating frame where small frequency drifts are compensated by applying $\mathbf{\Theta}$.

B. N_r equals N

Fig. 12 shows the experimental results obtained during the compensation process of the non-linear load by means of the analyzed SRF controllers. As can be seen in fig. 12.b there is a deviation from the load current consumption at the grid frequency. This is due to the fact that a portion of the load active power is supplied at the 5^{th} and 7^{th} harmonics. Once the SAPF is being operated properly, these harmonic currents must disappear from the source current spectrum. As a consequence, and in order to avoid the active power mismatch, the SAPF must increase the amplitude of the fundamental component

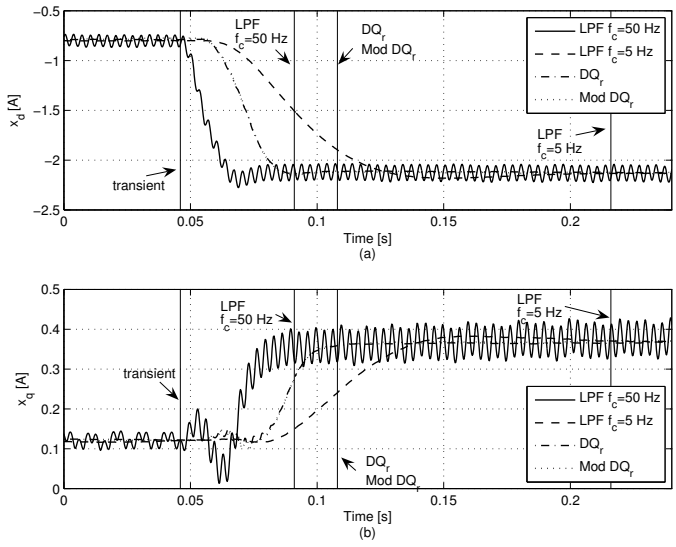

Fig. 13. Response to a load transient. a) d and b) q components of each SRF based controller

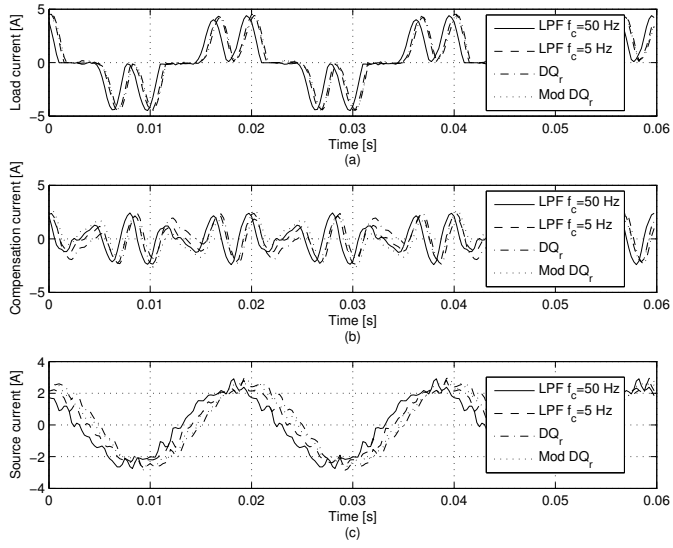

Fig. 14. Measured currents at the PCC at 50 Hz in phase A. a) load current b) compensation current and c) source current.

of the source current. The lowest deviation is measured for the $f_c = 50\ Hz$ LPF-based controller (4.1 %) and, as will be shown in fg. 12.c, this is due to an erroneous harmonic compensation which requires a lower active power to be supplied through the SAPF. It must be considered that the obtained experimental results differ from the simulation ones (fg. 5.b) due to the fact that in the first case only the electrical grid supplies power to the PCC but, in the second case and considering the SAPF as an ideal controllable current source, the power balance at the PCC can be also changed by the SAPF.

The measured source current is shown in fg. 12.c. As can be seen, all the analyzed methods compensate the 5^{th} and 7^{th} harmonics of the load current. The method involving the $f_c = 50\ Hz$ LPF exhibits the lowest performance, with 1.28 % and 6.74 % for these harmonics respectively.

A load transient has been applied by means of switch sw at $t = 0.046\ s$. The evolution of dq components for the SRF-implementations under test is shown in fg. 13.a and 13.b. As can be seen, the fastest response time corresponds to the LPF-based SRF method with $f_c = 50\ Hz$ (45 ms) while the slowest implementation is the LPF-based one with $f_c = 5\ Hz$ (170 ms). Both recursive implementations have equivalent response times (61 ms). The response time of the recursive implementations depends on the PCC voltage and current signal characteristics while the response times of LPF-based methods depend also on the low pass filtering stage characteristics.

The instantaneous values of the PCC currents in case $N_r = N$ (the grid frequency is 50 Hz) during the compensation process of the non-linear load current are shown in fg. 14. The initial load current has a THD equal to 70.3 %. Once the SAPF has reached the stationary state and, applying the LPF based methods with $f_c = 50\ Hz$ and $f_c = 5\ Hz$, the source current THD is reduced to 8.4 % and 4.3 % respectively. The difference between the reached THDs is due to characteristics

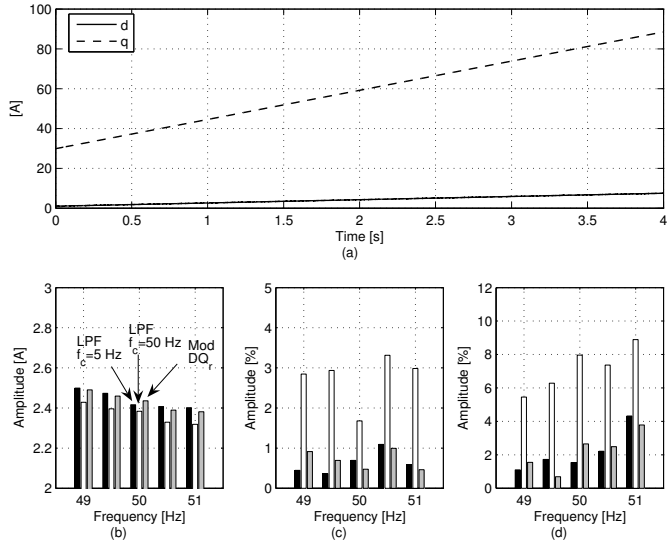

Fig. 15. Operation with $N_r \neq N$. a) dq components of the DQ_r controller with $f_{PLL} = 49\ Hz$, b) fundamental component of the source current in phase A, c) 5^{th} harmonic of the source current in phase A and d) 7^{th} harmonic of the source current in phase A. The test frequencies are 49, 49.5, 50, 50.5 and 51 Hz

of the applied LPF in each case. The DQ_r based controller and its modified version also reach low THDs, 4.2 % and 4.3 % respectively.

C. Different N_r and N

The SAPF controllers have been tested by applying grid voltage frequencies between the range $[49, 51]\ Hz$ with 0.5 Hz variations. Moreover, the resonance frequency of the current controllers have been changed during the tests in order to avoid their effect on the comparison. Fig. 15.a shows the dq components evaluated by the DQ_r method. As can be seen, due to $N_r \neq N$, the recursive implementation fails during the evaluation of the actual dq components of the load current.

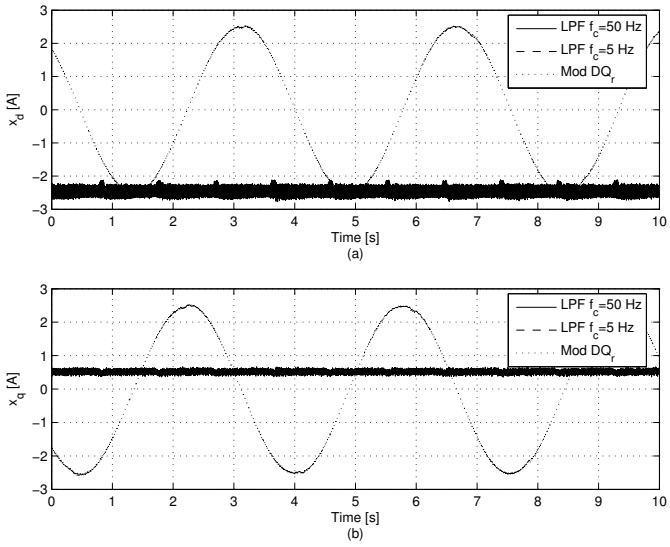

Fig. 16. Operation with $N_r \neq N$ at $f_{PLL} = 51\ Hz$. a) d and b) q components of the LPF and the modified DQ_r based methods

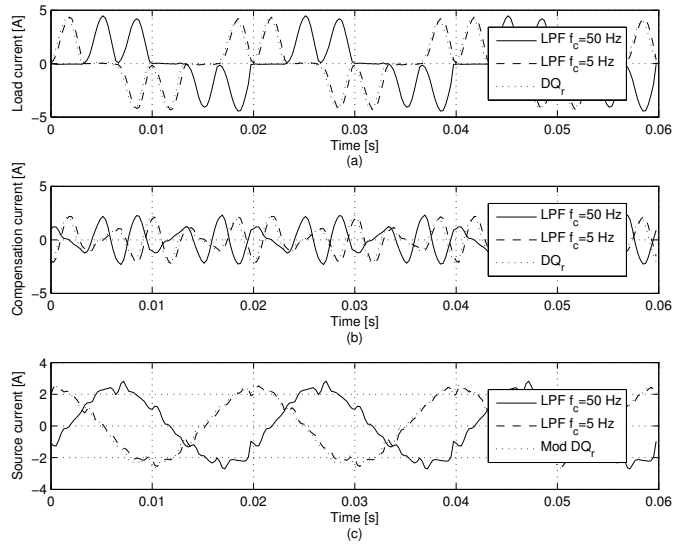

Fig. 17. Measured currents at the PCC at $51\ Hz$ in phase A. a) load current b) compensation current and c) source current

As a consequence, after the SAPF initialization, the overcurrent protection of the laboratory setup trips out and the SAPF is stopped. Hence, the operation of the SAPF prototype at frequencies in range [49,51] Hz has been tested with LPF-based controllers and the proposed modified recursive implementation.

Fig. 15.b shows the measured fundamental component of the source current with compensation at the test frequencies (49, 49.5, 50, 50.5 and 51 Hz). As can be seen, increasing the test frequency reduces the load current consumption and, as a consequence, the fundamental component of the source current. This effect is due to the fact that higher grid frequencies reduce the discharge transient of C while lower grid frequencies make this transient longer, which requires higher peak currents recharge this filtering capacitor^P. The current consumption of the LPF-based controller with $f_c = 50\ Hz$ is the lowest one in all tests, which is due to errors in harmonic compensation.

The relative amplitude of the measured 5^{th} and 7^{th} harmonics of the source current after compensation are shown in fig. 15.c and 15.d respectively. As can be seen, the LPF-based implementation with the lowest cut-off frequency and the proposed modified recursive implementation obtain similar results while the $f_c = 50\ Hz$ LPF-based controller can not compensate the load current harmonics properly.

The dq components evaluated by means of the tested SAPF controllers are shown in fig. 16. The programable power generator fed the non-linear load at $51\ Hz$ in order to obtain this figure. The LPF based methods obtain equivalent results as in the case of $N_r = N$. Small notches in dq components are due to the operation of the anti-windup protection associated to the dc-bus voltage controller (fig. 10). The modified DQ_r method generates a proper reference current for compensation purposes due to a second transformation to a rotating frame. From fig. 16, the period of the measured dq components is $3.55\ s$, which corresponds to $\frac{\omega_e}{2\pi} = 0.28\ Hz$, the frequency of the second rotating frame. The controller adjusted the length of Δ operators from 80 to 78 samples. In case of the DQ_r method, the overcurrent protection of the laboratory setup was tripped out while charging the dc-bus capacitor and, hence, the SAPF controller stopped the laboratory prototype.

The measured currents at the PCC, when the frequency of the programmable power source is $51\ Hz$ and the stationary state is reached, are shown in fig. 17. As it was previously discussed, the results associated to the DQ_r based controller are not depicted. The waveform of the source currents are quite similar in all the tested methods but the $f_c = 50\ Hz$ LPF based controller exhibits a higher ripple. The measured THDs reveal this effect. The initial load current THD is $72.1\ \%$ and, applying the laboratory prototype of SAPF, it is reduced to $10.1\ \%$, $5.7\ \%$ and $5.3\ \%$ by means of the LPF and modified DQ_r based controllers. As in previous cases, the best THDs are reached by employing a LPF stage with a low cutoff frequency and, equivalent results can be obtained by applying the proposed method. It must be considered that, in case of transients at the PCC and as it was shown in fig. 13, a low cutoff frequency results on a slower response time.

V. Conclusions

This paper proposes a recursive implementation of the Park Transformation which allows the improvement of SRF based controllers in shunt active power filters. Two recursive implementations, non-tolerant and tolerant to grid frequency variations, have been proposed and compared to LPF based implementations. A mathematical analysis, simulation tests and experimental results obtained on a laboratory prototype of SAPF are given. The obtained results demonstrate that the performance of LPF-based implementations depend on the PCC conditions and the filtering stage characteristics: controllers with low cut-off frequencies can be designed to obtain a good stationary state behavior but their response times to transients are high while controllers with high cut-off

frequencies have fast response times and low performance in stationary state. The proposed recursive implementation can be applied without considering the PCC conditions and avoids the design stage associated with LPF-based methods. Moreover, the obtained compensation results in stationary state and the measured response times to transients make the proposed method suitable for the development of improved SAPF controllers.

ACKNOWLEDGMENT

This work was partially supported by the Spanish Ministry of Science and Innovation under grant ENE2007-63979/ALT.

APPENDIX
FREQUENCY DOMAIN ANALYSIS OF $DQ_r - DQ^{-1}$ CONTROLLERS

The proposed $DQ_r - DQ^{-1}$ based controller can be analyzed in the frequency domain by applying Euler's formula to (11):

$$\begin{pmatrix} \hat{x}_d \\ \hat{x}_q \end{pmatrix}_k = \frac{1}{2N_r} \begin{pmatrix} a^k + a^{-k} & -j\left(a^k - a^{-k}\right) \\ j\left(a^k - a^{-k}\right) & a^k + a^{-k} \end{pmatrix} \cdot \begin{pmatrix} \Delta(x_\alpha) \\ \Delta(x_\beta) \end{pmatrix}_k + \begin{pmatrix} \hat{x}_d \\ \hat{x}_q \end{pmatrix}_{k-1} \tag{27}$$

where $a = e^{j\omega} = e^{j\frac{2\pi}{N}}$. Considering the property

$$\mathcal{Z}\left\{c^k f(k)\right\} = F\left(c^{-1}z\right), \tag{28}$$

it can be transformed to

$$\hat{x}_d(z) = \frac{\left(z^{N_r} - a^{N_r}\right)\left[x_\alpha\left(a^{-1}z\right) - jx_\beta\left(a^{-1}z\right)\right]}{2N_r\left(z^{N_r} - z^{N_r-1}\right)} + \frac{\left(z^{N_r} - a^{-N_r}\right)\left[x_\alpha(az) + jx_\beta(az)\right]}{2N_r\left(z^{N_r} - z^{N_r-1}\right)} \tag{29}$$

$$\hat{x}_q(z) = \frac{\left(z^{N_r} - a^{N_r}\right)\left[x_\beta\left(a^{-1}z\right) + jx_\alpha\left(a^{-1}z\right)\right]}{2N_r\left(z^{N_r} - z^{N_r-1}\right)} + \frac{\left(z^{N_r} - a^{-N_r}\right)\left[x_\beta(az) - jx_\alpha(az)\right]}{2N_r\left(z^{N_r} - z^{N_r-1}\right)} \tag{30}$$

The inverse DQ Transform in (4), employing Euler's Formula, can be represented as:

$$\begin{pmatrix} \hat{x}_\alpha \\ \hat{x}_\beta \end{pmatrix}_k = \frac{1}{2} \begin{pmatrix} a^k + a^{-k} & j\left(a^k - a^{-k}\right) \\ -j\left(a^k - a^{-k}\right) & a^k + a^{-k} \end{pmatrix} \begin{pmatrix} \hat{x}_d \\ \hat{x}_q \end{pmatrix}_k \tag{31}$$

and applying (28), it can be transformed to:

$$\hat{x}_\alpha(z) = \frac{1}{2}\left[\hat{x}_d\left(a^{-1}z\right) + \hat{x}_d(az) + j\hat{x}_q\left(a^{-1}z\right) - j\hat{x}_q(az)\right] \tag{32}$$

$$\hat{x}_\beta(z) = \frac{1}{2}\left[\hat{x}_q\left(a^{-1}z\right) + \hat{x}_q(az) - j\hat{x}_d\left(a^{-1}z\right) + j\hat{x}_d(az)\right] \tag{33}$$

Overall transfer functions for the proposed method can be obtained applying (29) and (30) to (32) and (33):

$$\hat{x}_\alpha(z) = \frac{\left(z^{N_r} - 1\right)\left[\left(z - cos\omega\right)x_\alpha(z) - sin\omega x_\beta(z)\right]}{N_r\left(z^{N_r+1} - 2cos\omega z^{N_r} + z^{N_r-1}\right)} \tag{34}$$

$$\hat{x}_\beta(z) = \frac{\left(z^{N_r} - 1\right)\left[\left(z - cos\omega\right)x_\beta(z) + sin\omega x_\alpha(z)\right]}{N_r\left(z^{N_r+1} - 2cos\omega z^{N_r} + z^{N_r-1}\right)} \tag{35}$$

REFERENCES

[1] H. Akagi, "Trends in active power line conditioners," *IEEE Transactions on Power Electronics,* vol. 13, no. 2, March 1994. pp. 263-268.

[2] T. C. Green and J. H. Marks, "Control techniques for active power filters," *IEE Proc. Electr. Power Appl.,* vol. 152, no. 2, March 2005. pp. 369-381.

[3] M. Sedighy, S. B. dewan and F. P. Dawson, "A robust digital current control method for active power filters," *IEEE Transactions on Industry Applications,* vol. 35, no. 4, July/August 2000. pp. 979-986.

[4] L. Asiminoaei, F. Blaabjerg and S. Hansen, "Evaluation of harmonic detection methods for active power filter applications," *Proc. of the IEEE* 20^{th} *Annual Aplied Power Electronics Conference and Exposition,* 6-10 March 2005, pp. 635-641.

[5] S.-J. Lee, H. Kim, S.-K. Sul and F. Blaabjerg, "A novel control algorithm for static series compensators by use of PQR instantaneous power theory," *IEEE Transactions on Power Electronics,* vol. 19, no. 3, May 2004. pp. 814-827.

[6] P. Salmerón and R. S. Herrera, "Distorted and unbalanced systems compensation within instantaneous reactive power framework," *IEEE Transactions on Power Delivery,* vol. 21, no. 3, July 2006. pp. 1655-1662.

[7] R. S. Herrera and P. Salmerón, "Instantaneous reactive power theory: A comparative evaluation of different formulations," *IEEE Transactions on Power Delivery,* vol. 22, no. 1, January 2007. pp. 595-604.

[8] O. F. Kashani and M. Braun, "Stability analysis of a compensated load on a grid to obtain unity power factor," *in Proc. of the 2005 European Conference on Power Electronics and Applications,* September 2005. 8 pp.

[9] V. M. Moreno and A. Pigazo, "Modified FBD method in active power filters to minimize the line current harmonics," *IEEE Transactions on Power Delivery,* vol. 22, no. 1, January 2007. pp. 735-736.

[10] J. M. M. Ortega, M. P. Esteve, M. B. Payan, A. G. Exposito and L. G. Franquelo, "Reference current computation methods for active power filters: accuracy assessment in the frequency domain," *IEEE Transactions on Power Electronics,* vol. 20, no. 2, March 2005. pp. 446-456.

[11] I. Etxeberria-Otadui, A. López de Heredia, H. Gaztaaga, S. Bacha and M. R. Revero, "A single synchronous frame hybrid multifrequency controller for power active filters," *IEEE Transactions on Industrial Electronics,* vol. 53, no. 5, October 2006. pp. 1640-1648.

[12] M. I. Milanés Montero, E. Romero Cadaval and F. Barrero González, "Comparison of control strategies for shunt active power filters in three-phase four-wire systems," *IEEE Transactions on Power Electronics,* vol. 22, no. 1, January 2007. pp. 229-236.

[13] M. El-Habrouk and M. K. Darwish, "Design and implementation of a modified Fourier analysis harmonic current computation technique for power active filters using DSPs," *IEE Proc. Electr. Power Appl.,* vol. 148, no. 1, January 2001. pp. 21-28.

[14] S. Mariethoz and A. C. Rufer, "Open loop and closed loop spectral frequency active filtering," *IEEE Transactions on Power Electronics,* vol. 17, no. 4, July 2002. pp. 564-573.

[15] J. Barros and E. Pérez, "An adaptive method for determining the reference compensating current in single-phase shunt active power filters," *IEEE Transactions on Power Delivery,* vol. 18, no. 4, October 2003. pp. 1578-1580.

[16] V. M. Moreno, A. Pigazo and R. I. Diego, "Reference current estimation under distorted line voltage for control of shunt active power filters," *IEEE Transactions on Power Electronics,* vol. 19, no. 4, July 2004. pp. 988-994.

[17] D. N. Zmood, D. G. Holmes and G. H. Bode, "Frequency-domain analysis of three-phase linear current regulators," *IEEE Transactions on Industry Applications,* vol. 37, no. 2, March/April 2001. pp. 601-610.

[18] M. J. Newman, D. N. Zmood and D. G. Holmes, "Stationary frame harmonic reference generation for active filter systems," *IEEE Transactions on Industry Applications,* vol. 38, no. 6, November/December 2002. pp. 1591-1599.

[19] P. Mattavelli, "A closed-loop selective harmonic compensation for active filters," *IEEE Transactions on Industry Applications,* vol. 37, no. 1, January/February 2001. pp. 81-89.
[20] J. Allmeling, "A control structure for fast harmonics compensation in active filters," *IEEE Transactions on Power Electronics,* vol. 19, no. 2, March 2004. pp. 508-514.
[21] J.-C. Wu and H.-L. Jou, "Simplified control method for the single-phase active power filter," *IEE Proc. Electr. Power Appl.,* vol. 143, no. 3, May 1996. pp. 219-224.
[22] IEEE Std. 519-1992, *IEEE Recommended practices and requirements for harmonic control in electrical power systems,* April 12, 1993.
[23] F. Blaabjerg, R. Teodorescu, M. Liserre and A. V. Timbus, "Overview of control and grid synchronization for distributed power generation systems," *IEEE Transactions on Industrial Electronics,* vol. 53, no. 5, October 2006. pp. 1398-1409.
[24] L. G. Barbosa Rolim, D. Rodrigues da Costa, Jr. and M. Aredes, "Analysis and software implementation of a robust synchronizing PLL circuit based on the pq theory," *IEEE Transactions on Industrial Electronics,* vol. 53, no. 6, December 2006. pp. 1919-1926.
[25] X. Yuan, W. Merk, H. Stemmler and J. Allmeling, "Stationary-frame generalized integrators for current control of active power filters with zero steady-state error for current harmonics of concern under unbalanced and distorted operating conditions," *IEEE Transactions on Industry Applications,* vol. 38, no. 2, 2002. pp. 523-532.
[26] R. I. Bojoi, G. Griva, V. Bostan, M. Guerriero, F. Farina and F. Profumo, "Current control strategy for power conditioners using sinusoidal signal integrators in synchronous reference frame," *IEEE Transactions on Power Electronics,* vol. 20, no. 6, November 2005. pp. 1402-1412.
[27] L. Asiminoaei, C. Lascu, F. Blaabjerg and I. Boldea, "New current control structure for shunt active power filters," *Proc. of the IEEE* 41^{st} *IAS Annual Meeting,* October 2006. pp. 183-190.
[28] P. Lezana, C. A. Silva, J. Rodríguez and M. A. Pérez, "Zero-steady-state-error input-current controller for regenerative multilevel converters based on single-phase cells," *IEEE Transactions on Industrial Electronics,* vol. 54, no. 2, April 2007. pp. 733-740.
[29] D. Sera, T. Kerekes, M. Lungeanu, P. Nakhost, R. Teodorescu, G. K. Andersen and M. Liserre, "Low-cost digital implementation of proportional-resonant current controllers for PV inverter applications using delta operator," *Proc. of the* 32^{nd} *Annual Conference of the IEEE Industrial Electronics Society,* November 2005. 6 pp.
[30] D. G. Holmes and T. A. Lipo, *Pulse width modulation for power converters. Principles and practice,*. IEEE Press, 2003.

Alberto Pigazo (M'05) received the M.Sc. and the Ph.D. degrees in Physics (Electronics) from the University of Cantabria, Spain, in 1997 and 2004 respectively. Since October 2000, he has been teaching courses of electronics, power electronics and digital signal processing at the Dept. of Electronics and Computers of the same university where he is currently an Assistant Professor. Dr. Pigazo has been a visiting researcher and professor at the Polytechnic of Bari, Italy, and he is member of the IES Technical Committee on Renewable Energy Systems (TCRES). He is also an Associate Editor of IEEE Industrial Electronics Magazine (IEM) and contributes as author and reviewer for IEEE journals and conferences.

Víctor M. Moreno (M'01) received the M.Sc. and the Ph.D. degrees in Physics (Electronics) from the University of Cantabria, Spain, in 1980 and 1994 respectively. His Ph.D. thesis, entitled "Distributed Measurement and Analysis System for Power Quality in Electrical Grids Applying Kalman Filtering", received the Viesgo Award in 1994. Dr. Moreno is an Associate Professor at the Dept. of Electronics and Computers, University of Cantabria, Spain and teaches electronics, power electronics, and signal processing techniques at the School of Nautical Studies, University of Cantabria. He is member of the IEEE Power Electronics Society (PELS) since 2001 and contributes as an author and reviewer for IEEE journals and conferences.

Emilio J. Estébanez received the M.Sc. degree in Telecommunications Engineering (Radiocommunications) from the University of Cantabria (Spain) in 2007. He is currently working as a researcher in the project ENE2007-63979/ALT "Islanding detection algorithms for low-voltage grid-connected inverters in photovoltaic distributed generation systems according to the EU standards (IDAPhoS)".